

Indexed by

Scopus®

EVALUATION OF STRUCTURAL RESPONSE OF COMPOSITE STEEL-CONCRETE ECCENTRICALLY BUCKLING-RESTRAINED BRACED FRAMES

DOAJ
DIRECTORY OF
OPEN ACCESS
JOURNALS

Crossref

Alireza Bahrami

Department of Building
Engineering, Energy Systems,
and Sustainability Science,
Faculty of Engineering and
Sustainable Development,
University of Gävle, Gävle,
Sweden

Mahmood Heidari

Department of Civil Engineering,
Abadan Branch,
Islamic Azad University,
Abadan, Iran

ROAD
DIRECTORY OF OPEN ACCESS
RESEARCH RESOURCES

KoBSON

Department of Civil
Engineering, Abadan Branch,
Islamic Azad University,
Abadan, Iran

SCINDEKS
Srpski citatni indeksGoogle
Scholar

Key words: buckling-restrained braced frame, composite, concrete, steel, lateral displacement, base shear, energy dissipation, dynamic analysis

doi:10.5937/jaes0-25497

Cite article:

Bahrami, A., & Heidari, M. [2020]. Evaluation of structural response of composite steel-concrete eccentrically buckling-restrained braced frames. *Journal of Applied Engineering Science*, 18(4), 591 - 600.

Online access of full paper is available at: www.engineeringscience.rs/browse-issues

EVALUATION OF STRUCTURAL RESPONSE OF COMPOSITE STEEL-CONCRETE ECCENTRICALLY BUCKLING-RESTRAINED BRACED FRAMES

Alireza Bahrami^{1,2*}, Mahmood Heidari²

¹Department of Building Engineering, Energy Systems, and Sustainability Science, Faculty of Engineering and Sustainable Development, University of Gävle, Gävle, Sweden

²Department of Civil Engineering, Abadan Branch, Islamic Azad University, Abadan, Iran

The main purpose of this paper is to evaluate the structural response of composite steel-concrete eccentrically buckling-restrained braced frames (BRBFs). The finite element (FE) software ABAQUS is employed to nonlinearly analyse the BRBFs. Comparing the modelling and experimental test results validates the FE modelling method of the BRBF. Three different strong earthquake records of Tabas, Northridge, and Chi-Chi are selected for the nonlinear dynamic analyses. A BRBF is then designed having a shear link. Afterwards, the designed BRBF is analysed under the selected earthquake records using the validated modelling method. The lateral displacements, base shears, and energy dissipations of the frame and shear link rotations are achieved from the analyses of the BRBF. The results are compared and discussed. The obtained BRBF results are also compared with their corresponding steel eccentrically braced frame (EBF) results. It is concluded that the BRBF can generally accomplish the improved structural response compared with the EBF under the earthquake records. Meanwhile, the BRBF has larger base shear capacity than the EBF. Moreover, the BRBF dissipates more energy than the EBF.

Key words: buckling-restrained braced frame, composite, concrete, steel, lateral displacement, base shear, energy dissipation, dynamic analysis

INTRODUCTION

Buckling-restrained brace (BRB) is one of the latest advances in lateral-resistant structures. The BRB has been implemented in structures throughout the world to prevent them from earthquake damages. The characteristic feature of the BRB is the buckling-restrained behaviour provided by encasing a steel core inside a buckling restraint system. However, research projects have suggested different ways of doing so over the years. In common braces, buckling of the brace against compressive forces is the cause of reducing its stiffness and strength which impedes the proper nonlinear behaviour of the structure and thereby decreases the ductility. Strengthening the brace against buckling increases its ductility and allows it to behave similarly against tensile and compressive forces. The BRB is an elastoplastic energy dissipater that is used to control the deformations resulting from lateral loads on the structure. The BRB dissipates most of the earthquake energy by a slender member protected against buckling. A typical BRB has a yielding steel core and a concrete-filled steel tube to prevent buckling of the core. It also includes end joints to connect the BRB to the building steel frame which creates the composite steel-concrete eccentrically buckling-restrained braced frame (BRBF).

The link length is an important issue in the design of the BRBFs and steel eccentrically braced frames (EBFs). Short and long links have shear and flexural failures, respectively. Studies have demonstrated bet-

ter performance of the short links than long links. The link length is limited to equation (1) in order to have the shear failure prior to flexural failure, accordingly, it is called a shear link. However, if the link length meets the requirement of equation (2), it is a moment link.

$$e < \frac{1.6 M_p}{V_p} \quad (1)$$

$$e > \frac{2.6 M_p}{V_p} \quad (2)$$

where e , M_p and V_p are the link length, plastic moment capacity, and plastic shear capacity of the link section, respectively.

On the other hand, if the link length is between the ranges of equations (1) and (2), it has simultaneous flexural-shear failure and is a moment-shear link.

Many research efforts have been directed towards the BRBs. A tube was utilised as a lateral support to prevent an axially loaded steel rod from buckling by Hollander [1]. The BRB has been used to avoid buckling of the traditional brace under earthquakes since the 1970s. Wakabayashi et al. [2] performed tests on BRBs applying different de-bonding materials between the brace and the buckling-restraint unit to decrease the friction. The practical application of BRBs was first achieved by Watanabe et al. [3]. Since then, the BRBs have widely been employed in tall buildings worldwide [4]. The design of the BRB as a damper to dissipate seismic energy was pro-

posed by Wada et al. [5]. Sabelli et al. [6] presented the seismic response of three- and six-storey concentrically braced frames using BRBs. Ju et al. [7] experimentally examined the load carrying capacity of BRBs composed of an H-shaped core element and an external tube. The contact force between the core and external restraining members was assessed by Jiang et al. [8] to investigate the performance of BRBs. The seismic behaviour of reinforced concrete (RC) structures retrofitted with BRBs was evaluated by Yang et al. [9] through testing two single-bay and three-storey RC frames specimens. An experimental research was carried out by Tsai et al. [10] on a BRB with inspection windows which allowed direct observation of the conditions of internal components of the BRB. Jia et al. [11] studied self-centring dual-steel BRBs consisting of a low-yield-point steel and a high strength steel. Hysteretic response of BRBs having various core materials, steel, and aluminium alloy and with various end connections was numerically examined by Avci-Karatas et al. [12]. Sadeghi and Rofooei [13] assessed the seismic performance of diagrids equipped with BRBs. The optimal design of steel BRBs against global buckling was done by Pan et al. [14]. Wang et al. [15] proposed a BRB with a gap-supported tendon protection in parallel. Zhu et al. [16] presented a study on the load carrying capacity and design method for a shuttle-shaped truss-confined BRB.

However, the investigation such as the current study on the evaluation of BRBFs under three different earthquake records of Tabas, Northridge, and Chi-Chi is rare which is offered herein.

This paper concentrates on the evaluation of the structural response of composite steel-concrete eccentrically BRBFs. The nonlinear dynamic analyses are conducted using the FE software ABAQUS. The validation of the BRBF modelling is carried out by comparing its result with the experimental test result. Thereafter, a BRBF is designed having a shear link. The validated modelling method is utilised for the analyses of the designed BRBF under three different earthquake records of Tabas, Northridge, and Chi-Chi. The results of the analyses are demonstrated as the lateral displacements, base shears, and energy dissipations of the frame and shear link rotations. The obtained BRBF results are compared and discussed. Also, the BRBF results are compared with their corresponding EBF results.

EXPERIMENTAL TEST

To validate the FE modelling, an experimentally tested BRB [17] was modelled in this study. In the experimental testing, the length and cross-sectional area of the steel core were 100 cm and 6.4 cm², respectively. The tube dimensions were 120 × 120 × 3 mm. Material properties of the steel and concrete are summarised in Tables 1 and 2, respectively. Cyclic loading was applied to the specimen based on the recommended provisions in FEMA 450 [18]. The test setup is shown in Figure 1. A 300 kN actu-

ator was used to conduct the test. As it can be observed from the figure, the test setup consisted of a hydraulic actuator, two end reaction blocks, a test specimen, and an auxiliary rigid member that facilitated the specimen fitting. Moreover, the figure illustrates the location of the global displacement instrumentation including two LVDTs placed at the end of the specimen. Strain gauges were also installed throughout the specimen to take the local instrumentation into account. Pinned connections were utilised. Figure 2 displays the test of the BRB.

Table 1: Material properties of steel core and tube

Component	Yield Stress (MPa)	Yield Strain	Ultimate Stress (MPa)	Ultimate Strain
Steel core	297.5	0.0022	449.8	0.21
Steel tube	370	0.0025	403.4	0.33

Table 2: Material properties of concrete infill

Component	Compressive Strength at 7 Days (MPa)	Compressive Strength at 28 Days (MPa)
Concrete	25	30

FE MODELLING

The solid element C3D8R was utilised to model the steel core and concrete infill of the specimen. Also, the shell element S4R was used for modelling the steel tube of the specimen. An essential part of the modelling was the material modelling which was carried out accurately. A bilinear steel material model was considered for modelling the steel having kinematic hardening behaviour. A concrete damage plasticity model was employed to model the concrete [19]. The same loading and boundary conditions as those of the tested specimen were adopted in the modelling. According to the applied convergence study on the mesh size of the model, the mesh size of 15 mm was found suitable for the analysis, because it could accomplish more accurate result. The results obtained from the convergence study are listed in Table 3.

Table 3: Results from convergence study

Mesh Size (mm)	Number of Elements	Maximum Tensile Force (kN)
15	7276	226.23
20	3869	219.78
30	1716	209.10
40	923	205.03
50	693	202.74
60	575	189.87

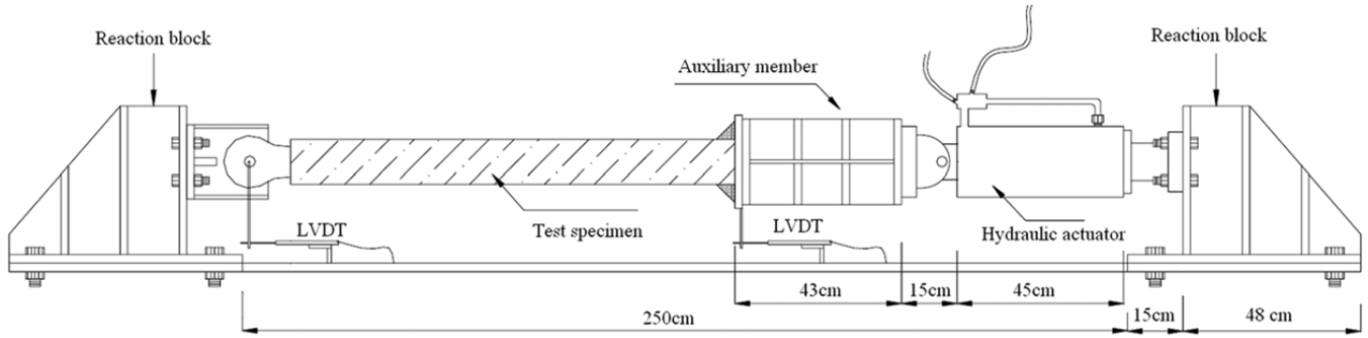


Figure 1: Test setup [17]



Figure 2: Test [17]

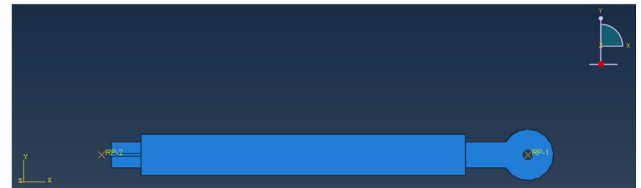


Figure 3: Modelled BRB

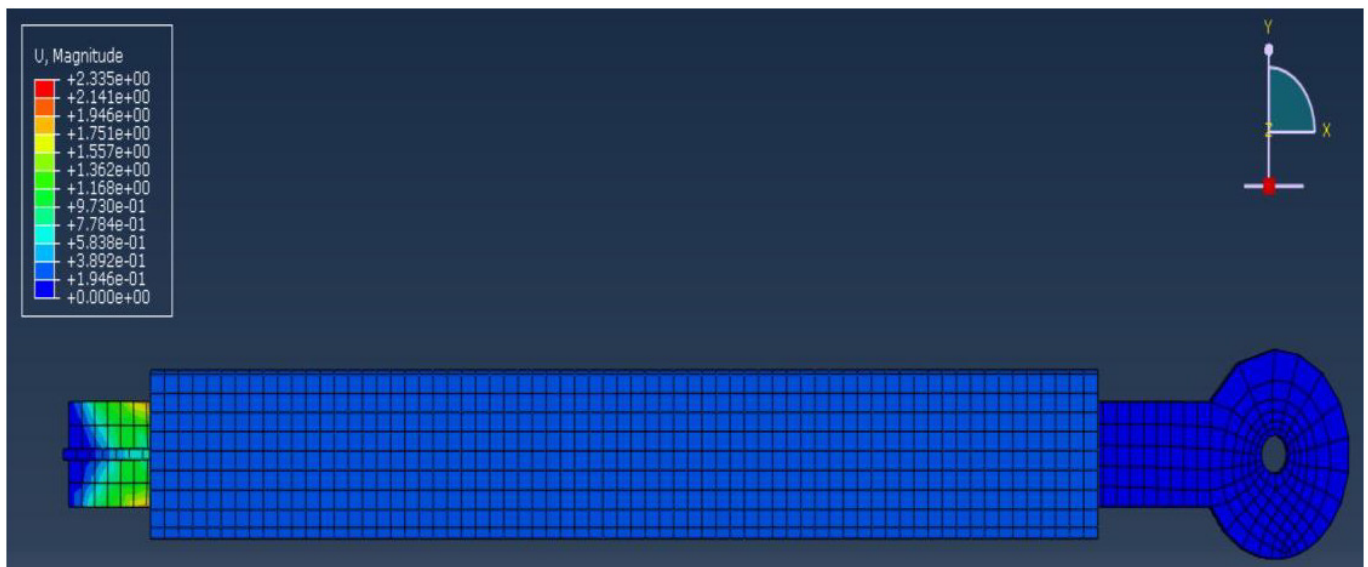


Figure 4: Stress distribution in modelled BRB with meshing

The aforementioned features of the tested specimen were all accounted for the modelling. The modelled BRB is indicated in Figure 3. Also, the stress distribution in the modelled BRB with meshing is elaborated in Figure 4.

The obtained result from the modelling is illustrated in the form of load-displacement plot. The modelling (ABAQUS) result of this study is compared with the results of the experimental test and numerical study [17] in Figure 5. Also, the maximum compressive and tensile forces achieved from the modelling (ABAQUS) are compared with those of the experimental test in Table 4. As can be witnessed from the table, the obtained maximum compressive and tensile forces from the modelling are a little different from their corresponding experimental test forces. These approximations are within the acceptable accuracy. Moreover, it can be seen from Figure 5 that the modelling (ABAQUS), experimental, and numerical curves lie close to each other. Therefore, it can be concluded from

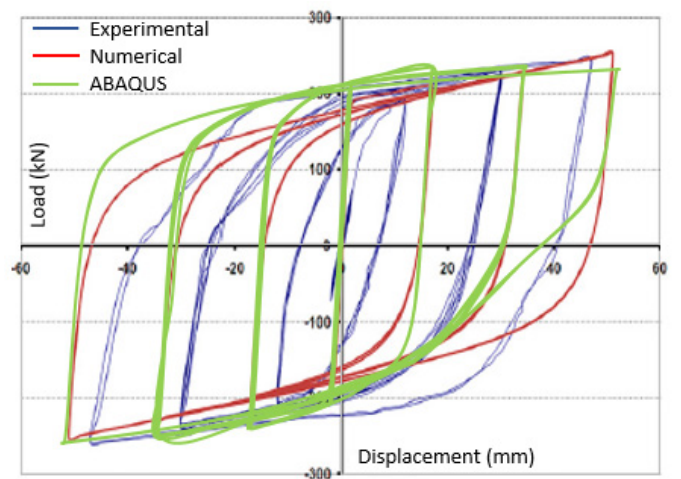


Figure 5: Comparison of modelling result (ABAQUS) with experimental and numerical results

Table 4: Comparison of maximum compressive and tensile forces from ABAQUS with experimental test

Force	Experimental Test Result E	ABAQUS Result A	A/E
Maximum compressive force (kN)	258	250.71	0.972
Maximum tensile force (kN)	243.28	226.23	0.930

the figure and table that the proposed FE modelling is completely able of predicting the response of the BRBs accurately. Hence, the modelling method was employed for further analyses of the BRBs in this research.

EARTHQUAKE RECORDS

To analyse the BRBF under the earthquake loading, three different accelerograms were selected. Specifications of these accelerograms are summarised in Table 5. M_w , PGA, PGV, and PGD are respectively as the magnitude of the earthquake, peak ground acceleration, peak ground velocity, and peak ground displacement.

Table 5: Specifications of earthquake records

Earthquake	Year	M_w (Richter Scale)	PGA (g)	PGV (cm/s)	PGD (cm)
Northridge	1994	6.70	0.349	32.25	9.30
Chi-Chi	1999	7.70	0.89	98	15.85
Tabas	1978	7.40	0.928	111.35	91.10

DESIGN OF BRBF

This section deals with the design of a BRBF having a shear link. Since the response of the BRBF is also compared with its corresponding EBF under the earthquake records in the current study, the BRBF was designed with the same geometrical dimensions of the EBF [20]. Thus, the height and width (L) of the specimen were

selected as 3150 mm and 3660 mm, respectively. The BRBF was designed with the shear link as the same as the EBF. Accordingly, the length of the shear links of the BRBF and EBF was 500 mm. The dimensions and spacing of the stiffeners in the link of the BRBF were also similar to those in the EBF. The loading on the BRBF was the above-mentioned earthquake records. The solid element C3D8R was utilised to model the steel core and concrete infill of the BRBF, and the shell element S4R was used to model the steel tube and other steel members of the BRBF. The columns ends supports were pinned. Figure 6 demonstrates the modelled BRBF. The BRBF was analysed dynamically under the selected records. The results of the analyses are presented in the following section.

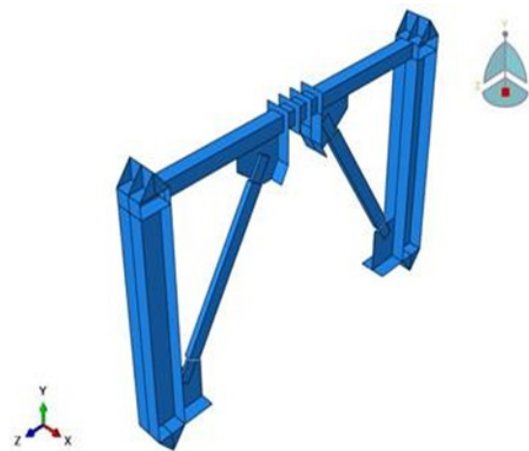


Figure 6: Modelled BRBF

RESULTS AND DISCUSSIONS

From the obtained results, the effects of the records as the lateral displacement, base shear, and energy dissipation of the frame and also the shear link rotation are discussed for the BRBF. Further, these results are compared with their corresponding results of the analysed EBF.

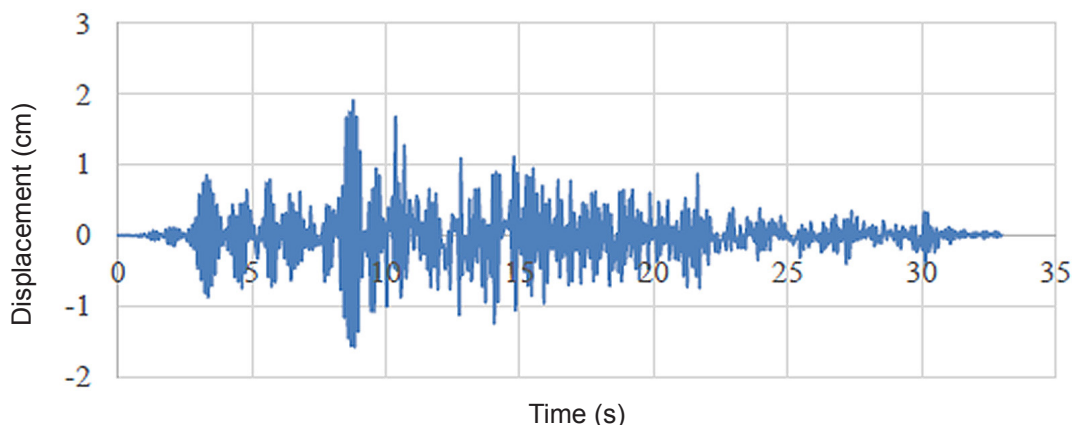


Figure 7: Lateral displacement of BRBF subjected to Tabas record

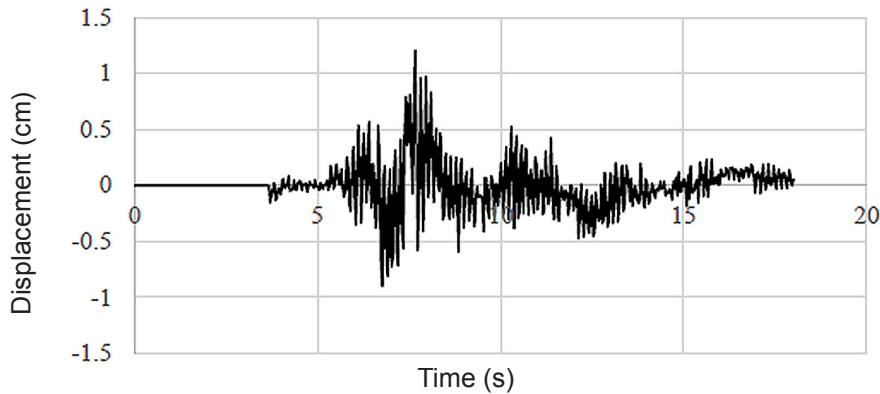


Figure 8: Lateral displacement of BRBF subjected to Chi-Chi record

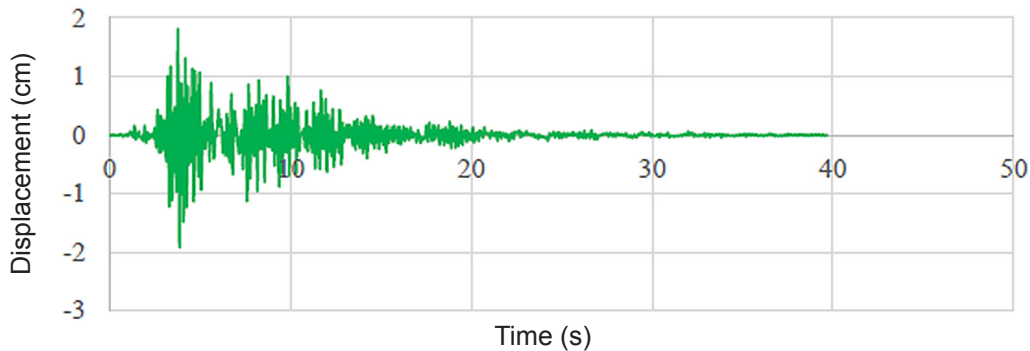


Figure 9: Lateral displacement of BRBF subjected to Northridge record

Lateral displacements

Figures 7-9 illustrate the achieved lateral displacement graphs from the analyses of the BRBF under the records. The maximum lateral displacements of the BRBF subjected to the records of Tabas, Chi-Chi, and Northridge are respectively as 1.9 cm, 1.2 cm, and 1.92 cm, as shown in Figure 10. Accordingly, the maximum lateral displacements of the BRBF under the Tabas and Northridge records are respectively 58.3% and 60% larger than that of the frame subjected to the Chi-Chi record. Meanwhile, it can be seen from Figure 10 that the lateral displacements of the BRBF are not directly proportional to the PGAs of their records, whilst, they are in a direct proportion for the EBF (Figure 11). On the other hand, the results in Figure 11 elaborate that if the BRBF is used, the lateral displacement of the frame is reduced. It is due to the higher stiffness of the BRBF than the conventional EBF which increases the overall stiffness of the system and reduces the lateral displacement of the frame. It should be noted that only the maximum lateral displacement of the BRBF under the Northridge record is slightly larger than that of the EBF. It is because of the point that many variables can also influence the dynamic behaviour of structures such as the ratio of the structure frequency to the earthquake frequency, the far or near fault record used, the record duration, and the earthquake energy. Consequently, many uncertainties are involved in the dynamic behaviour of structures under earthquake loadings that make the structural response against these variables unpredictable.

Base shears

The obtained base shear graphs of the BRBF subjected to the records are displayed in Figures 12-14. The difference of the maximum base shears of the frame subjected to the Tabas (9361 kN) and Chi-Chi (9203 kN) records is small. However, the maximum base shear of the frame under the Northridge record is 5298 kN. Therefore, the maximum base shears of the BRBF subjected to the Tabas and Chi-Chi records are respectively

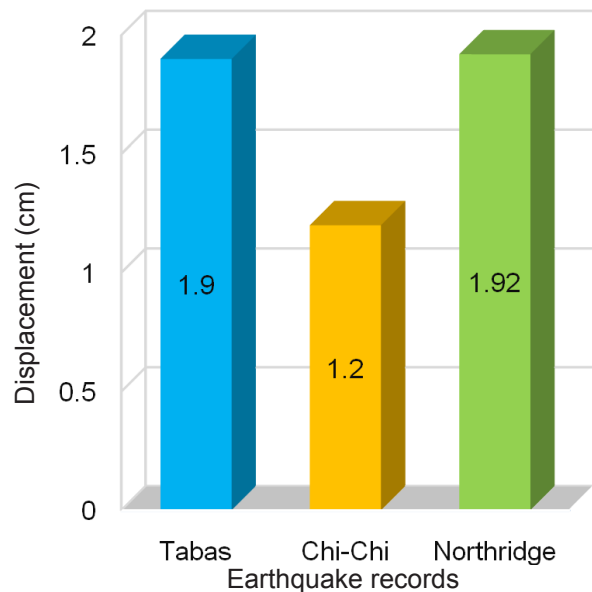


Figure 10: Comparison of maximum lateral displacements of BRBF subjected to different records

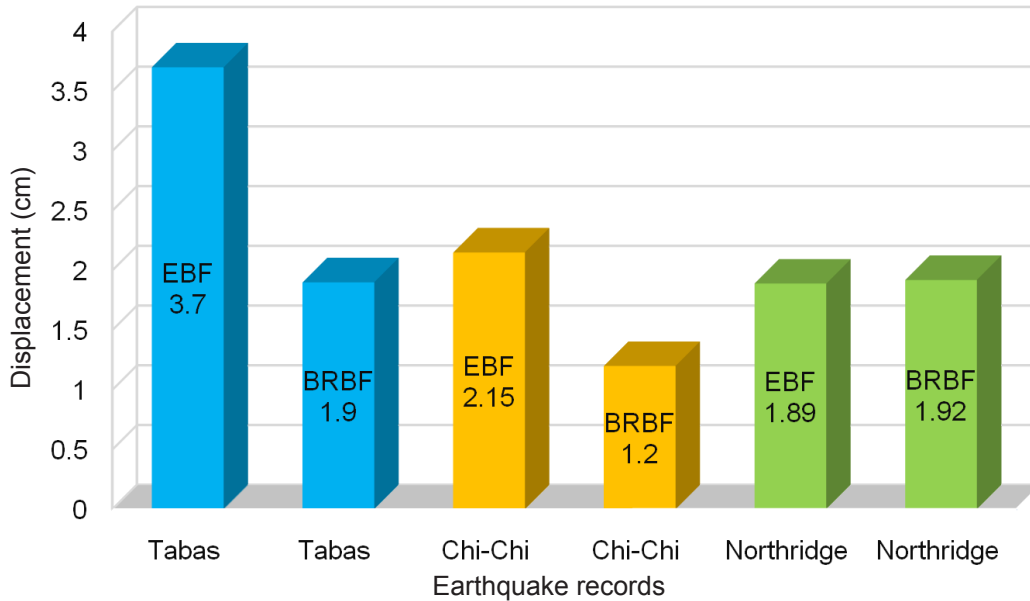


Figure 11: Comparison of maximum lateral displacements of BRBF and EBF subjected to different records

76.7% and 73.7% greater than that of the frame under the Northridge record (Figure 15). In addition, it can be witnessed from Figure 16 that the use of the BRBF increases the base shear capacity of the frame compared with the EBF. The reason for this issue can be attributed to the failure mode and the delay in starting the failure of the frame in the BRBF which makes the capacity of the structure more efficiently utilised.

Energy dissipations

Figures 17-19 show the energy dissipation graphs of the BRBF under the records. According to Figure 20, the maximum energy dissipations of the frame under the Tabas, Chi-Chi, and Northridge records are respectively as 201070 kN-cm, 23542 kN-cm, and 7440 kN-cm. Utilising

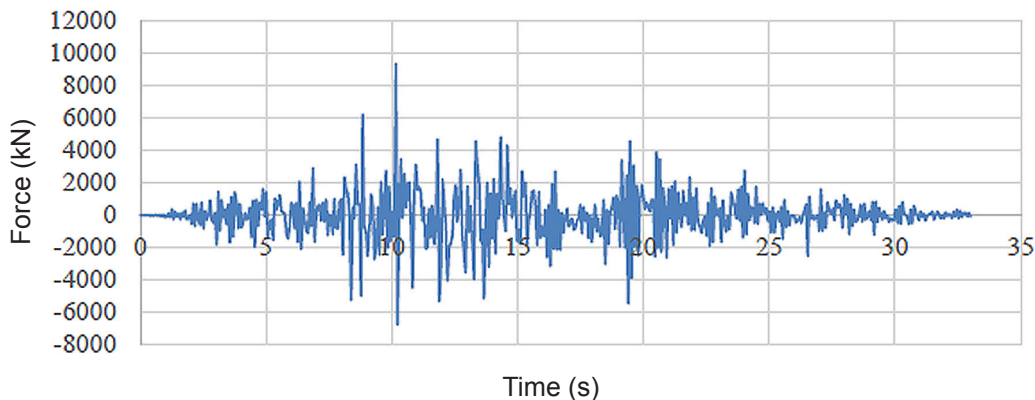


Figure 12: Base shear of BRBF subjected to Tabas record

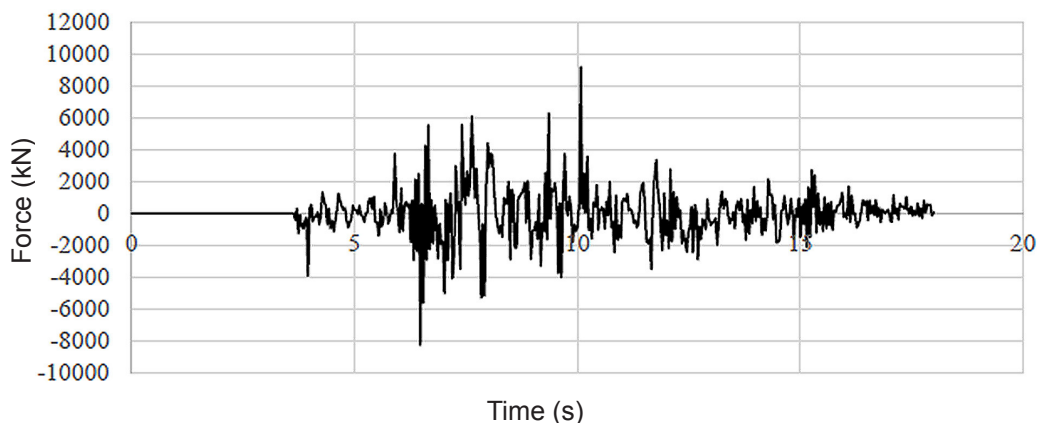


Figure 13: Base shear of BRBF subjected to Chi-Chi record

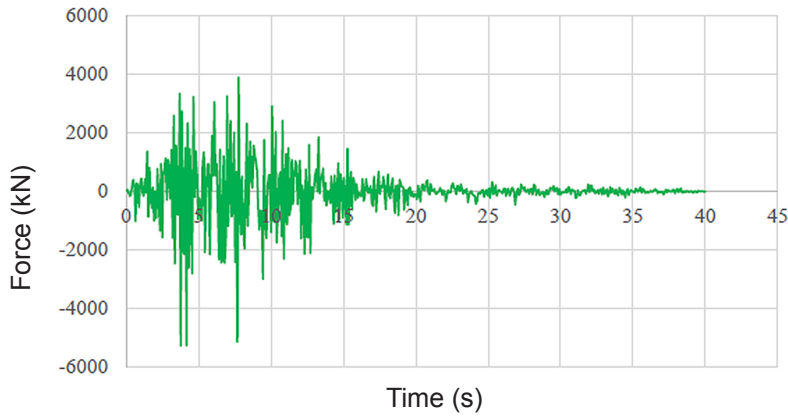


Figure 14: Base shear of BRBF subjected to Northridge record

the BRBF improves the energy dissipation of the frame compared with the EBF (Figure 21). Using the BRBF under the Tabas record has led to 79.4% more energy dissipation than employing the EBF.

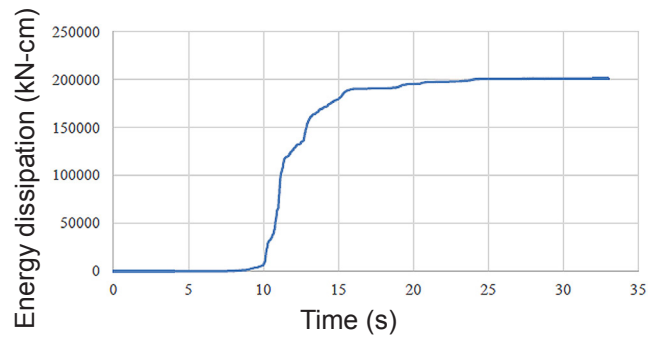


Figure 17: Energy dissipation of BRBF subjected to Tabas record

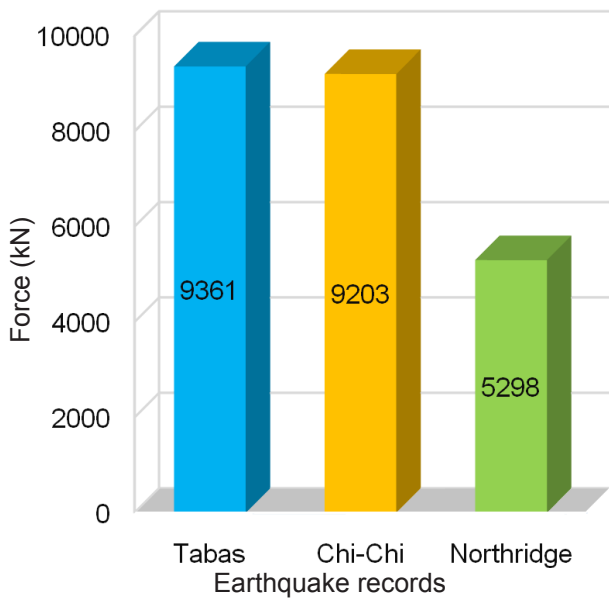


Figure 15: Comparison of maximum base shears of BRBF subjected to different records

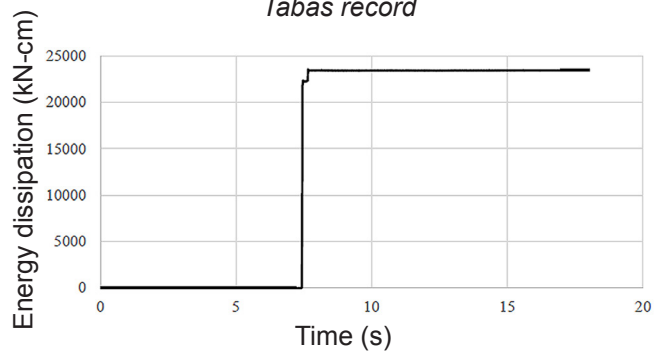


Figure 18: Energy dissipation of BRBF subjected to Chi-Chi record

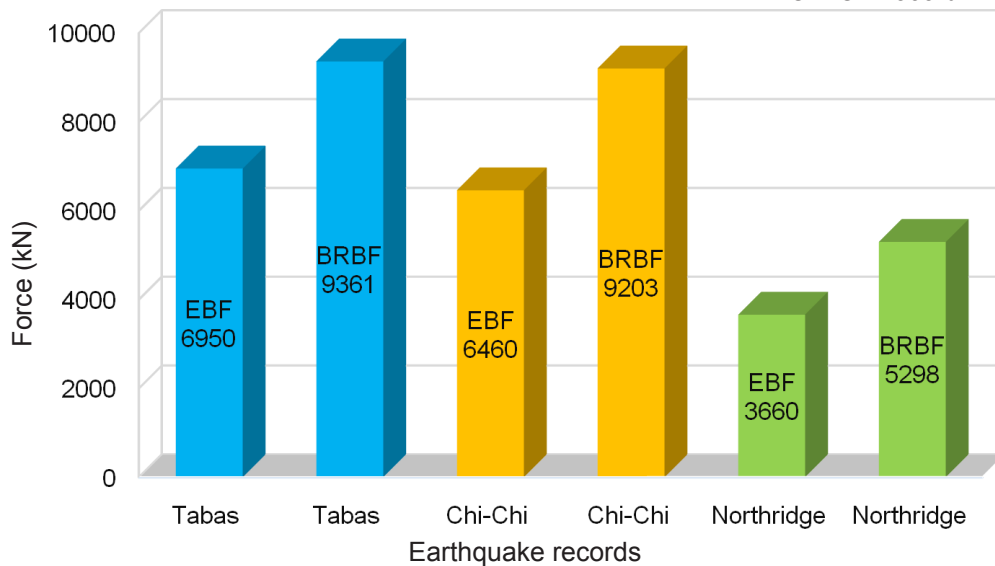


Figure 16: Comparison of maximum base shears of BRBF and EBF subjected to different records

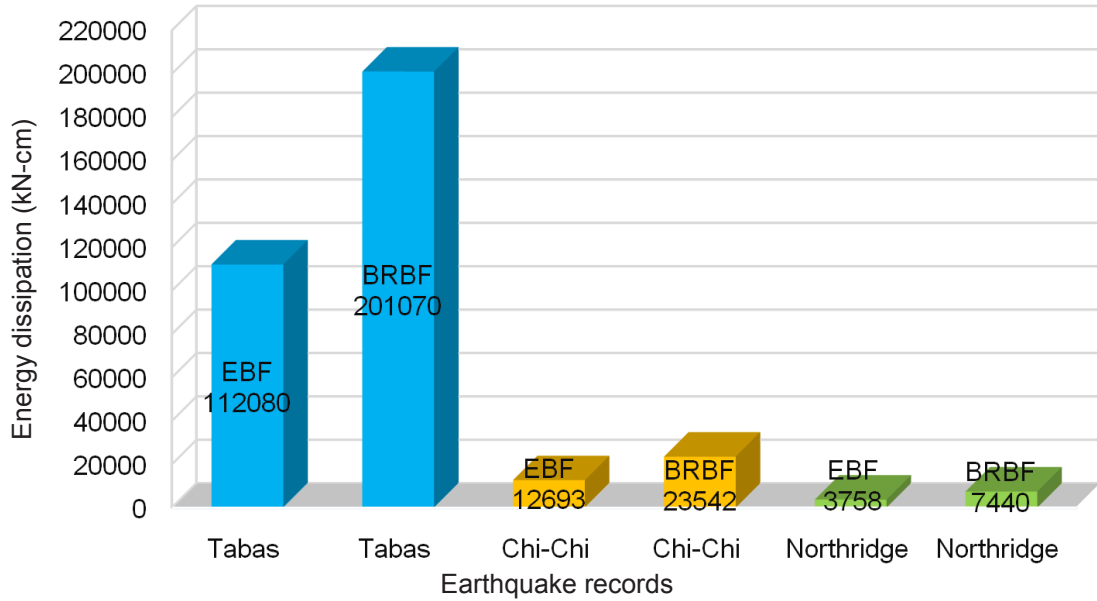


Figure 21: Comparison of maximum energy dissipations of BRBF and EBF subjected to different records

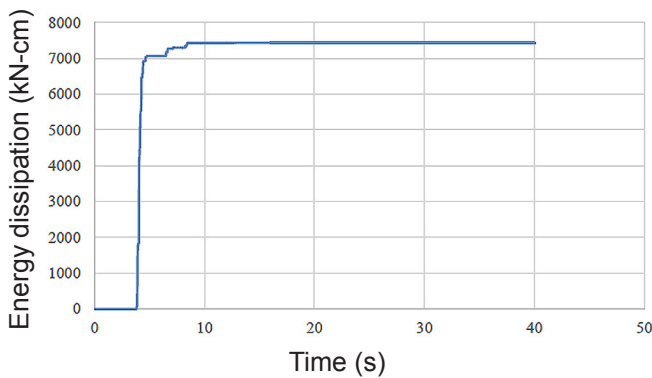


Figure 19: Energy dissipation of BRBF subjected to Northridge record

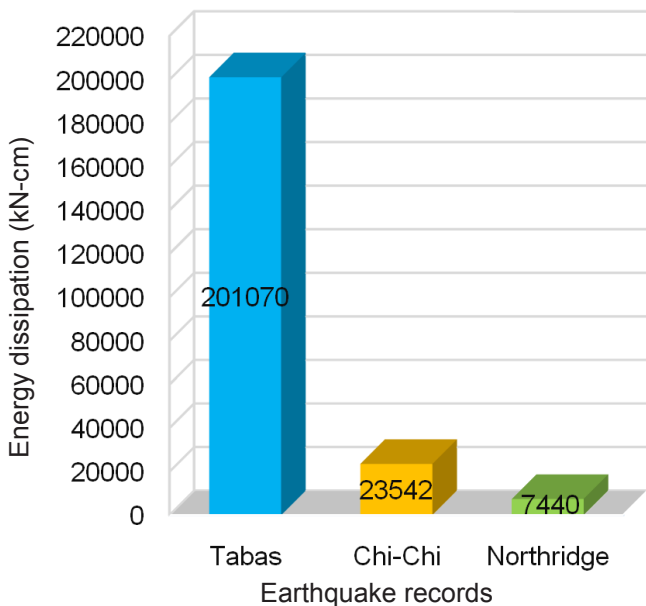


Figure 20: Comparison of maximum energy dissipations of BRBF subjected to different records

Rotations

Figure 22 presents the comparison of the maximum shear link rotations of the BRBF under the records. The rotations of the shear link were calculated by the use of equation (3):

$$\gamma = \frac{L}{e} \times \frac{\Delta}{h} \tag{3}$$

where L , e , Δ , and h are the width (frame span length), link length, frame lateral displacement, and frame height, respectively.

Since the link rotation is directly proportional to the lateral displacement of the frame and the hierarchy of the maximum lateral displacements of the frame under the earthquakes is Northridge, Tabas, and Chi-Chi, the same hierarchy can also be observed for the maximum

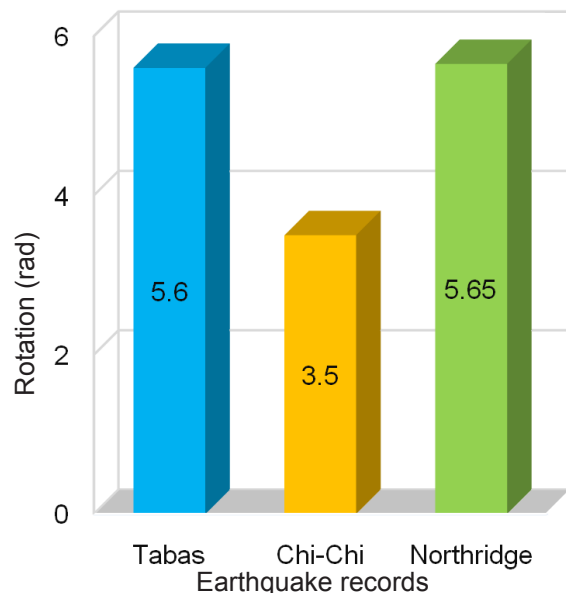


Figure 22: Comparison of maximum link rotations of BRBF subjected to different records

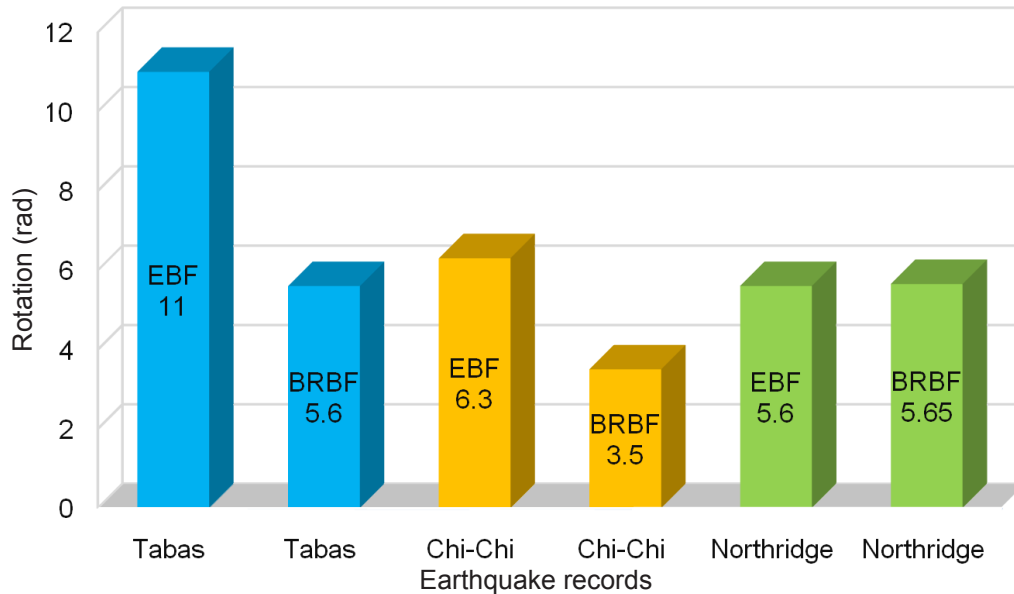


Figure 23: Comparison of maximum link rotations of BRBF and EBF subjected to different records

link rotations, as indicated in Figure 22. Comparing the maximum link rotations of the BRBF and EBF under different records in Figure 23 implies that utilising the BRBF decreases the link rotation compared with the EBF. The maximum link rotation of the BRBF under the Tabas record is about 2 times smaller than that of the EBF which emphasises the effectiveness of using the BRBF. However, the same point of the previously mentioned uncertainties in predicting the dynamic behaviour of structures under the earthquake loads can also be noticed herein for the maximum link rotations of the BRBF and EBF under the Northridge record which have a slight difference.

CONCLUSIONS

The structural response of the composite steel-concrete eccentrically BRBFs was examined under three different earthquake records. The analyses of the BRBFs were performed using the FE software ABAQUS. After validating the modelling of this study by comparison of its result with the experimental test result, a BRBF was designed having a shear link. The designed BRBF was then analysed under the selected earthquake records of Tabas, Northridge, and Chi-Chi. The obtained results from the analyses were displayed as the lateral displacements, base shears, and energy dissipations of the frame and shear link rotations. These results were compared and discussed, as well. The obtained BRBF results were also compared with their corresponding EBF results. Better structural response of the BRBF than the EBF was concluded for all the base shears and energy dissipations of the frame, and for most cases of the lateral displacements of the frame and also the shear link rotations. The BRBF provided greater base shear capacity and more energy dissipation than the EBF. Hence, a frame consisting of the BRB emerged as a practically effective option to resist the large lateral loads.

REFERENCES

- Hollander, M.B. (1966). Prestressed tubes and rods. US Patent No. 3232638.
- Wakabayashi, M., Nakamura, T., Kashibara, A., Morizono, T., Yokoyama, H. (1973). Experimental study of elasto-plastic properties of precast concrete wall panels with built-in insulating braces. Summaries of Technical Papers of Annual Meeting, Architectural Institute of Japan, Structural Engineering Section, vol. 10, 1041-1044, in Japanese.
- Watanabe, A., Hitomi, Y., Saeki, E., Wada, A., Fujimoto, M. (1988). Properties of brace encased in buckling-restraining concrete and steel tube. Proceeding of 9th World Conference on Earthquake Engineering, vol. IV, 719-724, Tokyo, Japan.
- Watanabe, A. (2018). Design and applications of buckling-restrained braces. International Journal of High-Rise Buildings, vol. 7, no. 3, 215-221.
- Wada, A., Connor, J., Kawai, H., Iwata, M., Watanabe, A. (1992). Damage tolerant structures. Proceeding of 5th U.S.-Japan Workshop on the Improvement of Structural Design and Construction Practices, Applied Technology Council, ATC-15-4, 27-39, San Diego, CA.
- Sabelli, R., Mahin, S., Chang, C. (2003). Seismic demands on steel braced frame buildings with buckling-restrained braces. Engineering Structures, vol. 25, no. 5, 655-666.
- Ju, Y-K., Kim, M.H., Kim, J., Kim, S.D. (2009). Component tests of buckling-restrained braces with unconstrained length. Engineering Structures, vol. 31, no. 2, 507-516.

8. Jiang, Z., Guo, Y., Zhang, B., Zhang, X. (2015). Influence of design parameters of buckling-restrained brace on its performance. *Journal of Constructional Steel Research*, vol. 105, 139-150.
9. Yang, Y., Liu, R., Xue, Y., Li, H. (2017). Experimental study on seismic performance of reinforced concrete frames retrofitted with eccentric buckling-restrained braces (BRBs). *Earthquakes and Structures-An International Journal*, vol. 12, no. 1, 79-89.
10. Tsai, C.S., Liu, Y., Liu, B.Q. (2017). An experimental study of buckling restrained brace with inspection windows. *Proceeding of 16th World Conference on Earthquake*, Santiago Chile, 1231.
11. Jia, L-J., Li, R-W., Xiang, P., Zhou, D-Y., Dong, Y. (2018). Resilient steel frames installed with self-centering dual-steel buckling-restrained brace. *Journal of Constructional Steel Research*, vol. 149, 95-104.
12. Avci-Karatas, C., Celik, O.C., Ozmen Eruslu, S. (2019). Modeling of buckling restrained braces (BRBs) using full-scale experimental data. *KSCE Journal of Civil Engineering*, vol. 23, 4431-4444.
13. Sadeghi, S., Rofooei, F.R. (2020). Improving the seismic performance of diagrid structures using buckling restrained braces. *Journal of Constructional Steel Research*, vol. 166, 105905.
14. Pan, W.H., Tong, J.Z., Guo, Y.L., Wang, C.M. (2020). Optimal design of steel buckling-restrained braces considering stiffness and strength requirements. *Engineering Structures*, vol. 211, 110437.
15. Wang, C-L., Qing, Y., Wu, J., Wang, J., Gu, Z. (2020). Analytical and experimental studies on buckling-restrained brace with gap-supported tendon protection. *Journal of Constructional Steel Research*, vol. 164, 105807.
16. Zhu, B-L., Guo, Y-L., Zhou, P., Pi, Y-L. (2020). Load-carrying performance and design of BRBs confined with longitudinal shuttle-shaped-trusses. *Journal of Constructional Steel Research*, vol. 167, 105954.
17. Mirtaheri, M., Gheidi, A., Zandi, A.P., Alanjari, P., Rahmani Samani, H. (2011). Experimental optimization studies on steel core lengths in buckling restrained braces. *Journal of Constructional Steel Research*, vol. 67, 1244-1253.
18. FEMA 450, (2003). NEHRP Recommended provisions for seismic regulations for new buildings and other structures, Part 1: provisions. Prepared by the building seismic safety council for the Federal Emergency Management Agency.
19. Bahrami, A., Yavari, M. (2019). Hysteretic assessment of steel-concrete composite shear walls. *International Journal of Recent Technology and Engineering*, vol. 8, no. 2, 5640-5645.
20. Bahrami, A., Heidari, M. (2020). Dynamic analysis of steel eccentrically braced frames with shear link. *International Journal of Engineering Research and Technology*, vol. 13, no. 2, 233-239.

Paper submitted: 01.03.2020.

Paper accepted: 18.08.2020.

*This is an open access article distributed under the
CC BY 4.0 terms and conditions.*